Lateral behavior of monopiles in sand under monotonic loading
Insights and a new simple design model

Wang, H.; Lehane, B. M.; Bransby, M. F.; Wang, L. Z.; Hong, Y.; Askarinejad, A.

DOI
10.1016/j.oceaneng.2023.114334

Publication date
2023

Document Version
Final published version

Published in
Ocean Engineering

Ocean Engineering 277 (2023) 114334

Contents lists available at ScienceDirect

Ocean Engineering

journal homepage: www.elsevier.com/locate/oceaneng

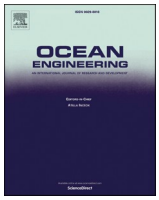

Lateral behavior of monopiles in sand under monotonic loading: Insights and a new simple design model

H. Wang [a,b,*], B.M. Lehane [c], M.F. Bransby [c], L.Z. Wang [d], Y. Hong [d], A. Askarinejad [a]

[a] Faculty of Civil Engineering and Geosciences, Delft University of Technology, the Netherlands
[b] Advanced Modelling Section, Norwegian Geotechnical Institute, Oslo, 0484, Norway
[c] The University of Western Australia, Crawley, WA, Australia
[d] College of Civil Engineering and Architecture, Zhejiang University, Hangzhou, China

ARTICLE INFO

Handling Editor: Prof. A.I. Incecik

Keywords:
Offshore wind turbines
Monopiles
Sands
Lateral load
Pile-soil interaction
Stiffness

ABSTRACT

This paper presents a synthesis of recent and new research conducted by the authors on laterally loaded monopiles in drained sand. The research involved reduced-scale field tests, centrifuge model tests, finite element (FE) simulations and comparisons of design approaches with published experimental data. The influence of the monopile base on lateral response is first discussed by drawing on field tests and numerical simulations and it is shown that the base generally provides a negligible contribution. The applicability of the API *p-y* formulation is then investigated through systematic FE analyses. The results show that this formulation leads to inaccurate predictions largely due to the assumption of a high initial stiffness varying linearly with depth and an unrealistic hyperbolic tangent back-bone function. Based on new insights into pile-soil interaction together with elastic simulations of laterally loaded rigid piles and new observations based on 26 pile tests, a simple rotational spring model is proposed to allow rapid quantification of the non-linear response of rigid monopiles in uniform sand. The effect of monopile flexibility is then added through a new straightforward correction factor based on 80 extra FE simulations. Finally, an example application of the proposed approach for a typical monopile design is presented.

1. Introduction

Piles are commonly used to support offshore infrastructure that is subjected to large lateral and moment loading (e.g. Fleming et al., 2008; Doherty and Gavin, 2012; Negro et al., 2017; Houlsby, 2016). For jacket structures used in the oil and gas industry, piles with diameters (D) less than about 2 m and lengths (L) typically greater than 50 m are employed to resist applied moments in a 'push-pull' mode. These piles usually have an aspect ratio (L/D) of 30 or more and respond in a flexible way in bending with near zero lateral movement below a certain depth, see Fig. 1a. In contrast, single (or mono) piles with diameters of 5 m, and more, and L/D ratios less than 5 are the preferred foundation for offshore wind turbines (Negro et al., 2017). These piles are stiff in bending and may be expected to undergo rigid body rotation when subjected to large lateral loads (as shown in Fig. 1b). Consequently, large movements are developed at the pile base, accompanied by the potential to mobilise significant resisting base shear force and moments.

For the analysis of laterally loaded piles, the most popular design approach is the *p-y* load transfer method, where p is lateral soil reaction (in force per unit length) and y is pile deflection at a given depth. In this method, the pile is modelled as beam elements, while the soil is represented by non-interacting, nonlinear springs distributed along the pile length (Reese et al., 1974). The most widely used *p-y* formulation for piles in sand is that recommended by the American Petroleum Institute (API, 2011). This formulation, which was based primarily on results from a small number of lateral tests conducted in the field on flexible piles, has been used successfully for the design of small diameter offshore piles for many years. However, many recent studies suggest that the API formulation is not suitable for the design of large diameter rigid monopiles (DNV, 2014; Thieken et al., 2015; Klinkvort, 2012; Choo and Kim, 2015). Some researchers (Lam and Martin, 1986; Ashour and Helal, 2013; Byrne et al., 2015) contest that the inaccuracies in predictions obtained with the API *p-y* model arise because the approach ignores the contribution provided at the base of the monopile. However,

* Corresponding author. Faculty of Civil Engineering and Geosciences, Delft University of Technology, the Netherlands.
E-mail addresses: H.Wang-16@tudelft.nl, huan.wang@ngi.no (H. Wang), barry.lehane@uwa.edu.au (B.M. Lehane), fraser.bransby@uwa.edu.au (M.F. Bransby), wanglz@zju.edu.cn (L.Z. Wang), yi_hong@zju.edu.cn (Y. Hong), A.Askarinejad@tudelft.nl (A. Askarinejad).

https://doi.org/10.1016/j.oceaneng.2023.114334
Received 5 October 2022; Received in revised form 12 March 2023; Accepted 23 March 2023
Available online 1 April 2023

experimental investigations (Klinkvort, 2012; Alderlieste, 2011; Leth, 2013; Choo et al., 2014; Choo and Kim, 2015) and numerical studies (Wiemann et al., 2004; Sørensen, 2012; Wang et al., 2020) on large diameter monopiles show that the API (2011) formulation leads to over-prediction of a monopile's lateral stiffness. No conclusive consensus has been achieved on the suitability of the *p-y* load transfer method for monopiles and how *p-y* curves may scale with diameter. Furthermore, the resistance provided by the pile base has not been investigated systematically for a wide range of conditions.

This paper synthesizes a recently completed research programme conducted by the authors, adds new results, and includes observations from the public domain regarding laterally loaded monopiles undergoing monotonic loading in drained sand. The research addressed apparent inconsistencies in existing studies and involved reduced scale field tests, centrifuge model tests and finite element simulations. The major findings from the studies combined with observations from other relevant research projects are used here to address the following four key questions that are of significant importance for monopile foundation designers in the offshore wind industry:

(i) Does the pile base resistance matter?
(ii) Why does the conventional API *p-y* formulation not work for rigid piles in sand?
(iii) Is there an alternative simple design approach for rigid piles in sand?
(iv) What is the influence of flexural rigidity for a monopile?

2. Does the pile base resistance matter?

Before investigating why the conventional API *p-y* formulation does not work for monopiles in sand, it is important to first quantify the contribution of the pile base resistance (i.e., base shear force and base moment) to the lateral response and examine if the *p-y* load transfer method is still applicable to large diameter monopiles in drained sand. In this regard, Wang et al. (2022a) performed a unique series of field tests on 0.273 m and 0.457 m diameter, short pipe piles (L/D between 2.2 and 5.5) at the University of Western Australia (UWA) Shenton Park test site. The piles were installed by an air hammer and a fully coring was observed for all the piles after the installation. To examine explicitly the contribution of the pile base to the pile response under lateral load, four tests (L1, L2, S1, S2) were performed with the sand inside two of the piles (L1 and S1) removed carefully before lateral loading using a hand auger to a distance of at least 100 mm below their tips (as shown in Fig. 2). This operation ensured a zero contribution of base shear force and moment during the subsequent lateral load tests on these piles. In addition, two 0.273 m diameter model piles of 1.0 m and 1.5 m in length were instrumented with strain gauges to provide bending moment profiles that allowed derivation of the *p-y* curves, which were then employed in a beam-spring model to evaluate the applicability of the *p-y* load transfer method. Although the piles were not subjected to external axial loads, it should be noted that the load mobilized at the base of a monopile in service is small because the total axial load is resisted primarily in skin friction under working conditions.

The measured pile head load-deflection responses are presented in Fig. 3, while Fig. 4 compares these responses with those computed using the experimentally derived *p-y* curves. It is evident from Fig. 3 that the piles with and without the soil plug removed (i.e., without and with pile base shear force and moment contributions) exhibit virtually identical responses under lateral loading. The very small differences in the pile responses can be explained easily by natural variability in the sand at the site and minor experimental errors. It can be inferred that the contribution of base shear and moment to the lateral responses of the tested piles ($D = 0.273$ m and 0.457 m) is negligible. A negligible contribution from the pile base is supported by load-deflection curves calculated using *p-y* curves derived from the measured bending moment distributions on the 0.273 m diameter piles, as shown in Fig. 4. It is evident that without adding any additional base shear or moment springs, the *p-y* springs alone are sufficient to capture the lateral response of these piles. The *p-y* load transfer method is therefore suitable for these short piles, provided that appropriate *p-y* curves are employed.

The diameters of monopiles used offshore are significantly larger than those used at Shenton Park and are usually larger than 5 m. The applicability of the experimental observations for full-scale conditions was therefore investigated by Wang et al. (2022a) through a series of finite element (FE) analyses of wished-in-place piles under the conditions with and without sand plugs removed and employing the hardening soil constitutive model to represent the Shenton Park sand (Mathew and Lehane, 2012). Importantly, the FE model was first validated against the experimental results with good agreement being obtained, as shown in Fig. 5a, which plots the normalized lateral load, $H/\gamma' D^3$ (where H is force at the pile head, and γ' is the submerged unit weight of the soil) against normalized ground level lateral displacement, y/D. The calculated responses of large scale 30 m long monopiles employing the same constitutive parameters for the sand are presented

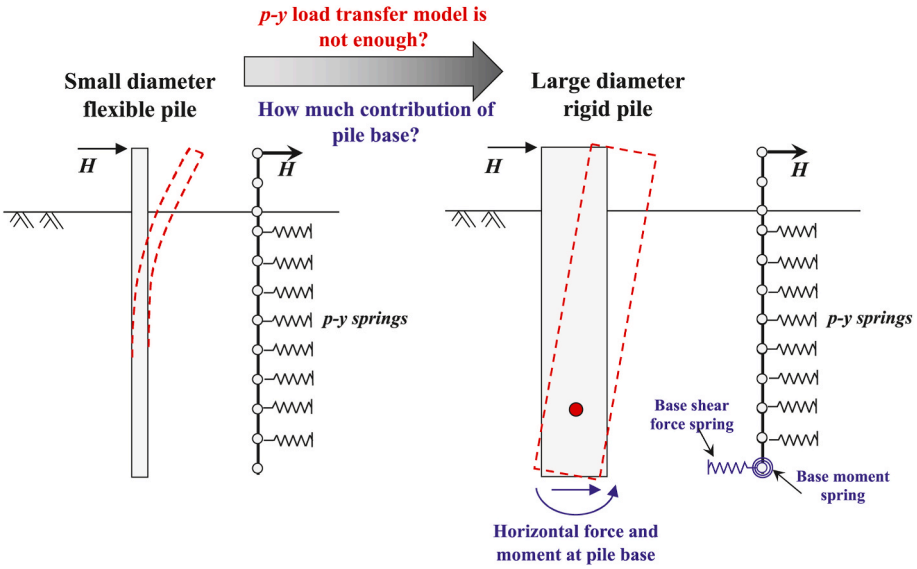

Fig. 1. Pile deflection response for (a) piles used in conventional jackets and (b) monopiles used for offshore wind turbines.

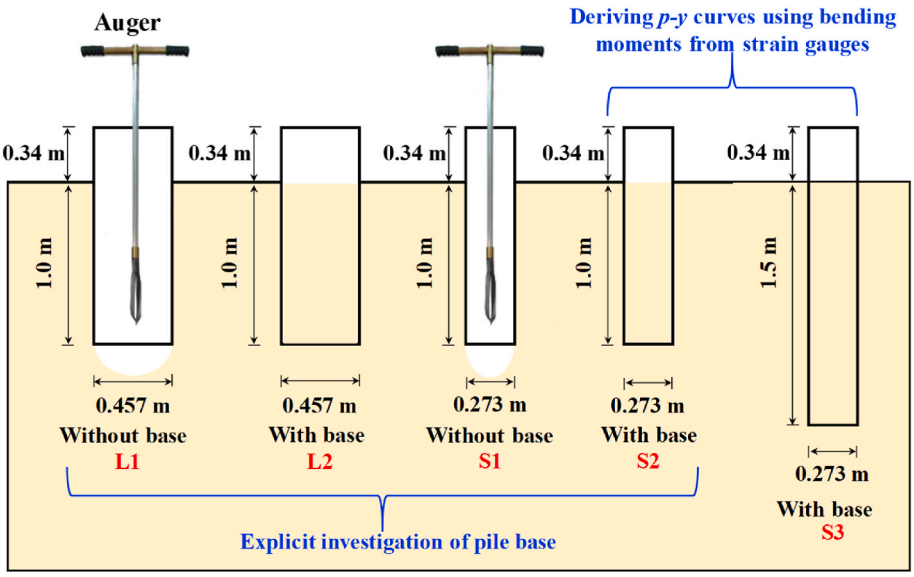

Fig. 2. Schematic of field tests conducted in Shenton Park sand to quantify the pile base influence and examine the *p-y* load transfer method for monopiles (Wang et al., 2022a).

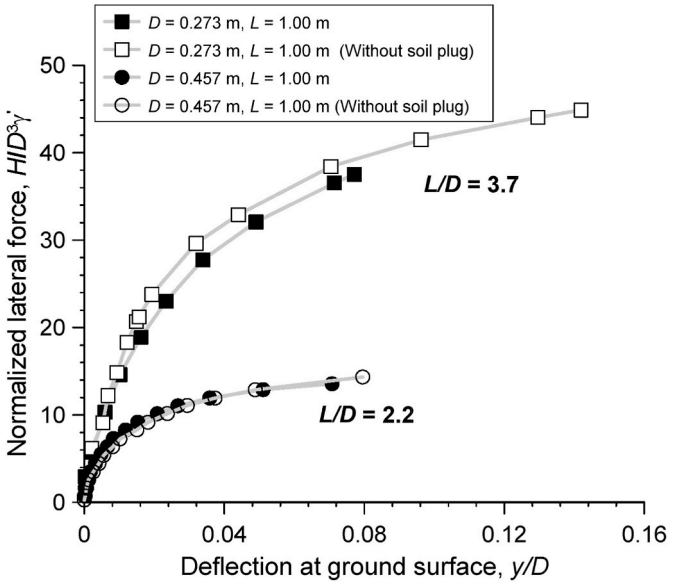

Fig. 3. Measured load–deflection response of piles with and without soil plug (Wang et al., 2022a).

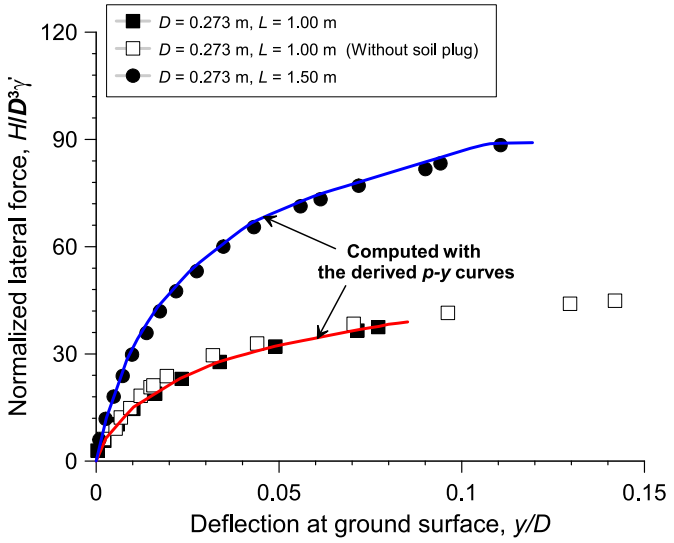

Fig. 4. Comparison of the measured load–deflection response and the computed with the experimentally derived *p-y* curves (Wang et al., 2022a).

in the same format on Fig. 5b and show that the 6 m diameter pile with no sand plug (and hence no base contribution) responds in a near identical manner to the pile with a sand plug (and hence with the potential to mobilise base resistance). A similar observation was reported in Byrne et al. (2015) based on numerical simulations on a 10 m diameter and 20 m length monopile in sand.

Although a slight difference (around 10%) in predicted responses are seen on Fig. 5b for the 10 m diameter monopile, these analyses combined with the findings from Shenton Park and other existing studies (Murphy et al., 2018; Byrne et al., 2015) clearly indicate that the base resistance has a negligible effect on the lateral response of a monopile. The agreement seen between measured pile responses at Shenton Park and those calculated using the *p-y* approach on Fig. 4 also shows that poor predictions obtained using the API *p-y* formulation (mentioned above) cannot be attributed to the exclusion of base resistance components in the approach.

3. Why the conventional API *p-y* model does not work for rigid piles in sand?

Given that the diameter of monopiles is about one order of magnitude larger than that used in the derivation of the API *p-y* formulation (Reese et al., 1974), some studies argue that the inaccuracy of the API approach arises because of a dependence of *p–y* curves on pile diameter (Carter, 1984; Wiemann et al., 2004; Kallehave et al., 2012; Sørensen, 2012). In contrast, other studies report little influence of pile diameter (Ashford and Juirnarongrit, 2003; Klinkvort, 2012; Klinkvort and Page, 2014; Finn and Dowling, 2015). However, as an increase in pile diameter is accompanied by an increase in pile bending stiffness, it is possible that differing views regarding the 'diameter effect' may result from the mixed effects of pile diameter and pile rigidity (Carter, 1984; Pender, 2004; Fan and Long, 2005; Liang et al., 2007; Jeong et al., 2011; Finn and Dowling, 2015).

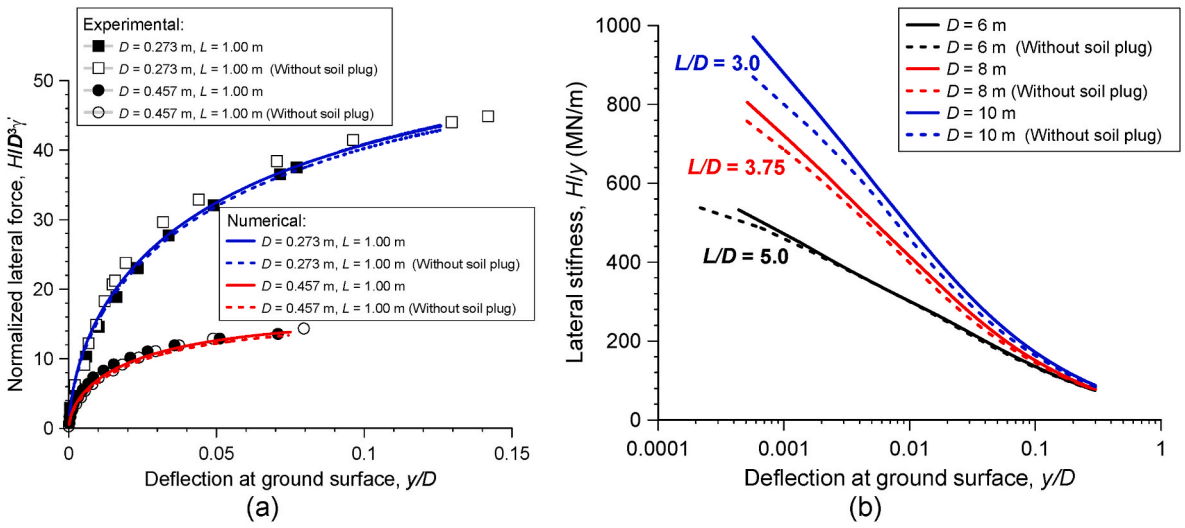

Fig. 5. Load-deflection response at ground surface: (a) validation of the finite element pile-soil model though comparison with field data; (b) response of large diameter monopiles as calculated using FEA (Wang et al., 2022a).

3.1. *Effect of pile diameter on p-y response*

To isolate the effects of diameter on soil-pile interaction, Wang et al. (2022b) performed a unique series of finite element (FE) simulations on four different diameter monopiles (D = 4, 6, 8, 10 m). The monopiles have the same length (L) of 30 m and a very high Young's modulus to ensure a fully rigid response under lateral load. The hypoplastic sand model with intergranular strain was adopted to model the nonlinear and state-dependent behavior of sand. Triaxial element tests under different stress paths (Hong et al., 2016) and centrifuge pile tests in medium dense Toyoura sand (Wang et al., 2022b) were performed to calibrate the sand model and validate the FE pile-soil model.

Computed pile-soil interaction results are summarized in Fig. 6 together with the calculated results using the API *p-y* formulation. It is evident that the API *p-y* model leads to much higher predictions of lateral stiffness for all diameter monopiles compared with the numerical analyses. This observation is in keeping with the findings of experimental studies reported by Georgiadis et al. (1992), Klinkvort (2012), Choo et al. (2014), Kirkwood (2016), Zhu et al. (2016) and Li et al. (2017) and of numerical analyses by Lesny and Wiemann (2006), Achmus et al. (2011), Thieken et al. (2015) and Amar Bouzid (2018). In fact, Georgiadis et al. (1992) and Zhu et al. (2016) found that the API *p-y* model overestimates the initial stiffness, even for small-diameter flexible piles at shallow depths. The high stiffness predicted by the API *p-y* formulation can be partly attributed to the assumption of a linear increase of initial stiffness with depth and the high subgrade coefficients recommended in Reese et al. (1974). Many existing studies (e.g. Poulos, 1971; Randolph, 1981; Pender, 2004; Wan et al., 2021) have shown that the initial lateral stiffness of *p-y* curves in any given soil horizon is related directly to the small strain (elastic) shear modulus (G_0). Therefore, the overestimation of stiffness will be further amplified for large diameter monopiles at higher stress levels (see comparisons in Fig. 6b) as the small-strain elastic G_0 value in a uniform sand varies with the stress level raised to a power of less than 1 (and is typically about 0.5).

3.2. *Effect of formulation for p-y back-bone function*

Another source for stiffness overestimation at small displacement is the hyperbolic tangent back-bone function adopted in the API model:

$$p = p_u \tanh\left[\frac{k_{ini}}{p_u} y\right] \tag{1}$$

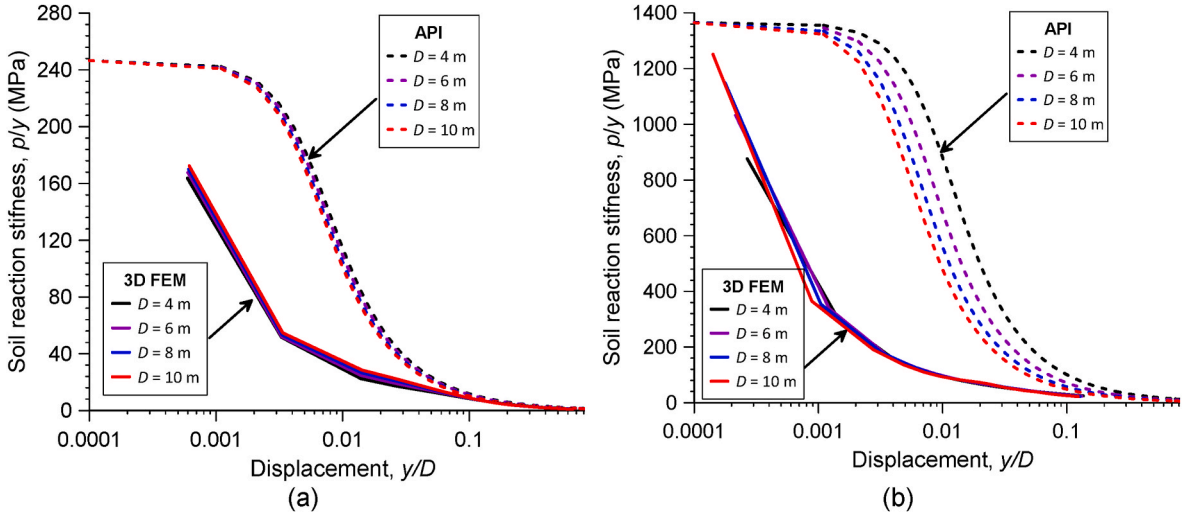

Fig. 6. *p/y–y/D* curves at depth: (a) z = 4·5 m; (b) z = 27 m (Wang et al., 2022b); (Note: the loading height is 5 m in FE simulations; the API *p-y* curves were calculated with the critical state friction angle of 31°).

where k_{ini} is the initial stiffness and p_u is the ultimate soil resistance.

To highlight this, the hyperbolic function adopted by many studies (e.g. Georgiadis et al., 1992; Klinkvort, 2012; Kirkwood, 2016; Choo and Kim, 2015; Zhu et al., 2016) is selected here for comparison:

$$p = \frac{y}{\frac{1}{k_{ini}} + \frac{y}{p_u}} \quad (2)$$

Fig. 7 compares the *p-y* curves calculated using the hyperbolic tangent function (Eq. (1)) in API and the hyperbolic function (Eq. (2)) adopted by recent studies with the same initial stiffness k_{ini} and ultimate soil resistance p_u (calculated from the API formulation using an effective soil weight of 10 kN/m^3 and friction angle of 31°). Even with the same inputs, the API *p-y* model leads to a much higher stiffness at small displacement and mobilises the ultimate soil resistance at a much lower displacement compared with the hyperbolic function (Eq. (2)) adopted in recent studies.

3.3. Net pressure distribution at ultimate lateral load

In addition, an important observation evident in Fig. 6 is that the FE-calculated *p/D–y/D* curves for the different pile diameters are in close agreement at each depth (i.e., z = 4.5 m and 27 m); this observation implies that the load transfer curves of monopiles in sand are a function of the depth below the ground surface (i.e., z) instead of the depth to diameter ratio (i.e., z/D) as assumed in the API model. Although it was not stated explicitly, the same observation of the dependency of the soil pressure on the absolute depth can be identified in the numerical simulations of the PISA project reported by Burd et al. (2020). This unique feature of monopiles in sand is further illustrated in Fig. 8 by plotting the lateral soil pressure at the ultimate lateral capacity for four different diameter rigid monopiles. The ultimate soil pressure calculated using the formulation in the API model is also presented in Fig. 8 for comparison. It is evident that the lateral pressure distribution at ultimate lateral load for rigid monopiles in uniform sand is independent of pile diameter and is function of absolute depth (z) or depth relative to the pile length (z/L) instead of the depth ratio (z/D) defined in API model (as shown in Fig. 8).

3.4. Failure mechanisms for rigid and flexible piles

The independence of the *p/D-y/D* curves (Fig. 6) and lateral pressures at ultimate load capacity (Fig. 8) is attributed to differences in the failure mechanisms of large diameter (rigid) monopiles and small diameter (flexible) piles. In the API model proposed for small diameter flexible piles, the sand resistance at shallow depth is governed by a wedge type failure mechanism in response to lateral soil movement induced by the pile; this mechanism transitions to a 'flow around' failure in the horizontal plane at depth (as shown in Fig. 9). However, as shown in Fig. 10, large diameter rigid monopiles undergo rotation under lateral loading. Monopiles of all diameters exhibit a deep wedge failure mode in the upper section of the pile with rotational soil flow in the vertical plane below this section (instead of in the horizontal plane presumed in the API model). As shown in Fig. 8, the lateral pressure increases with depth in the upper wedge zone but begins to reduce at z ≈ 0·5L as the point of rotation at z ≈ 0·75L is approached. It is evident from Fig. 10 that the depth separating the wedge zone and the rotational zone is the same for all pile diameters, which explains the independence of the ultimate lateral pressure distribution on diameter shown in Fig. 8. The mechanism illustrated in Fig. 10 was also identified by Murff and Hamilton (1993), Randolph et al. (1998) and Hong et al. (2017) for suction anchors and rigid piles in undrained clay subjected to lateral force and moment loading. A thorough review on the ultimate soil resistance of laterally loaded piles in sand is provided Wang et al. (2022d).

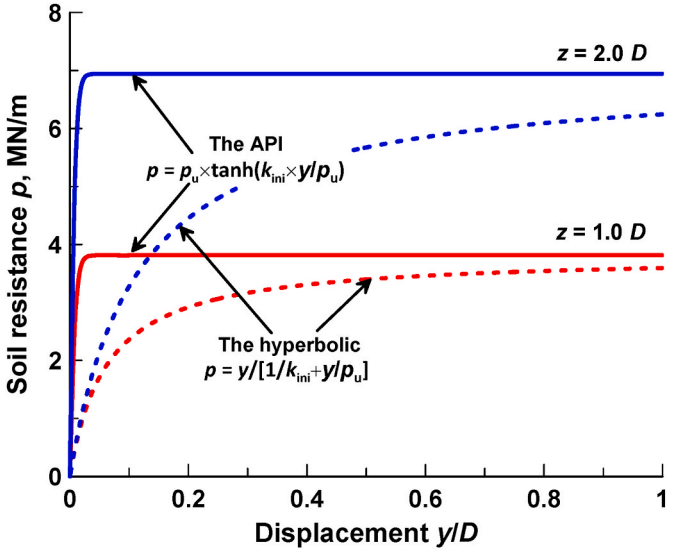

Fig. 7. The influence of back-bone function on the *p-y* curves (Note: the pile diameter D = 6 m).

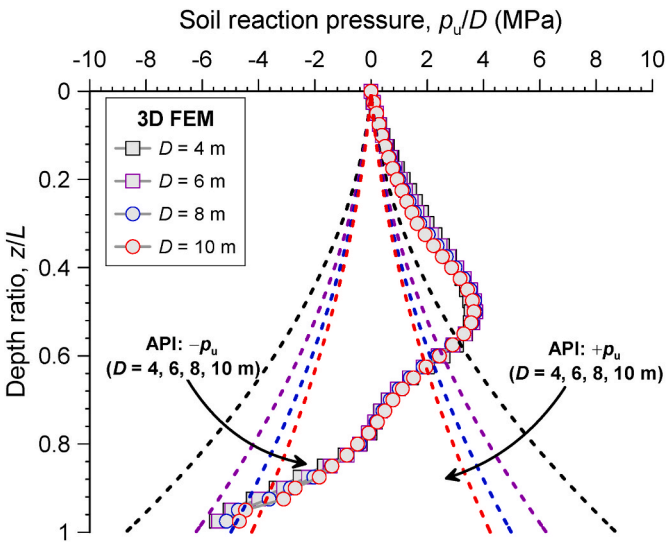

Fig. 8. Comparison of the lateral soil pressure (P_u) profiles between the FE computed at ultimate capacity and the calculated from API *p-y* model.

3.5. Effects of applied moment (or lateral load eccentricity)

Offshore wind turbine monopiles are subjected to the lateral loads from the combined actions of wind, wave and current. The foundations have to resist the horizontal force and large overturning moment simultaneously. Monotonic loading can therefore be represented by a single horizontal force acting at a (large) loading eccentricity (h). The effect of loading eccentricity on the pile-soil interaction of monopiles in sand was examined explicitly by Wang et al. (2022b) in a series of FE simulations involving a wide range of loading eccentricities (h = 5 m–100 m) and four monopile diameters (D = 4, 6, 8, 10 m); the hypoplastic model was used to model the sand (as employed for predictions presented above). Results from the study are summarized in Fig. 11 and clearly illustrate a negligible influence of loading eccentricity on the lateral stiffness ($p/y = P/(y/D)$, $P = p/D$) response of the sand. The net pressures at ultimate lateral load (P_u) were also found to be practically independent of the loading eccentricity. This observation was also confirmed by the centrifuge tests on the large diameter monopiles in Klinkvort and Hededal (2014) and Li et al. (2022).

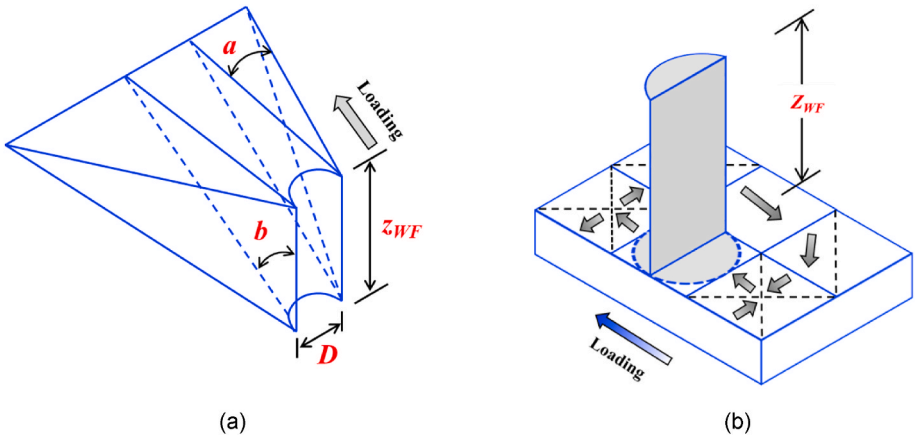

Fig. 9. The assumed failure mechanisms of the API *p-y* model in sand (Reese et al., 1974; Amar Bouzid, 2018).

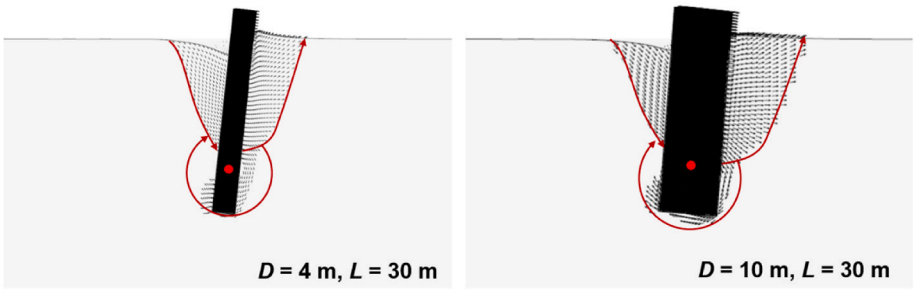

Fig. 10. Failure mechanism of the rigid monopiles in sand (Wang et al., 2022b).

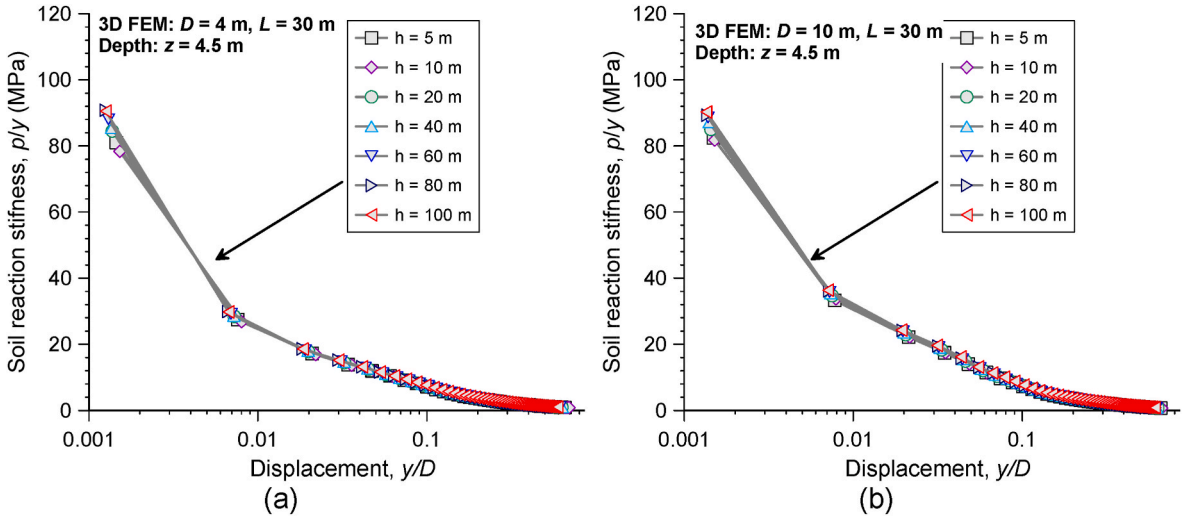

Fig. 11. Influence of loading eccentricity on pile-soil interaction: (a) *p/D–y/D* curves of 4 m diameter monopiles at depth $z = 4{\cdot}5$ m; (b) *p/D–y/D* curves of 10 m diameter monopiles at depth $z = 4{\cdot}5$ m.

3.6. Summary

The study presented in Figs. 6–11 has shown that API *p-y* model formulation is not suited to the prediction of the lateral response of monopiles because the specified initial stiffness and stiffness degradation characteristics (i.e., the adopted back-bone function) are not appropriate for the distinctly different mode of failure under applied lateral load and moment of rigid piles compared with flexible piles. The FE analyses reveal that the mode of failure of monopiles is such that both the *p/D-y/D* curves in any sand horizon and the net pressures at ultimate lateral capacity are independent of pile diameter and loading eccentricity.

4. Is there an alternative simple design approach for a rigid pile in sand?

4.1. Simple rotational spring model for rigid pile

The preceding sections have demonstrated that the contribution of the pile base to the lateral response of monopiles in sand is negligible for

the conditions investigated and revealed that the net lateral pressures at ultimate capacity are independent of the pile diameter and loading eccentricity due to the unique rotational failure mechanism of monopiles in drained sand. Based on the FE analysis, Wang et al. (2022b) demonstrates that the net pressure distribution shown on Fig. 12, where (away from the rotation point) pressures (P) are linearly proportional to the vertical effective stress (i.e., $P = p/D = K\sigma'_v = K\gamma' z$, where K is the soil pressure coefficient, which is function of the rigid pile rotation; For the value of K at ultimate state, i.e., K_{ult}, a detailed review can be found in Wang et al., 2022d). This is consistent with the mechanism of rigid piles in a uniform sand and with the model originally proposed by Petrasovits and Award (1972).

Following the simplified pile-soil interaction model in Fig. 12, moment equilibrium relative to the rotation center leads to the following expressions:

$$M_R = H(h+d) = \int_0^d KDz\gamma'(d-z)dz + \int_d^L KDz\gamma'(z-d)dz = KDL^3\gamma'\left[\frac{1}{3}\left(\frac{d}{L}\right)^3 - \frac{1}{2}\left(\frac{d}{L}\right) + \frac{1}{3}\right] \quad (3)$$

where d is depth of the rotation center, M_R is the over-turning moment relative to the rotation center.

Wang et al. (2022b) presents the results of numerical simulations involving rigid monopiles with a wide range of geometric configurations (D = 4–10 m, L/D = 3 to 7.5) and loading eccentricities (h = 5–100 m). These analyses confirm the suitability of the simplified pile-soil interaction model on Fig. 12 and show that the rotation center position is independent of pile diameter and loading eccentricity, and stabilizes at around 0.75L with a variation of less than 3%. Eq. (3) can be therefore simplified as:

$$M_R = H(h+0.75L) = KDL^3\gamma'\left[\frac{1}{3}(0.75)^3 - \frac{1}{2}(0.75) + \frac{1}{3}\right] \approx 0.1KDL^3\gamma' \quad (4)$$

Since the results in Figs. 6 and 8 have demonstrated the independence of lateral resistance (and so also the coefficient K) on pile diameter (D), Eq. (3) suggests that the lateral response of rigid monopiles in sand can be represented by the normalization $M_R/DL^3\gamma'$. In addition, Wang et al. (2022b) found that the simplified pile-soil interaction model in Fig. 12 holds not only for the ultimate state, but also at any rotation (for the hypoplastic constitutive model employed). Wang et al. (2022c) subsequently proposed that a laterally loaded rigid pile can be modelled as a beam hinged at a rotation center at a depth of 0.75L and constrained by a rotational spring, as shown in Fig. 12.

The validity of the rotational spring model is demonstrated in Fig. 13, which plots the normalized moment-rotation response about the rotation center at 0.75L. As shown in Fig. 13, for 4 m and 8 m diameter rigid monopiles, the lateral response under a wide range of loading eccentricities (h = 5–100 m) can be perfectly represented by a single $[M_R/\theta DL^3\gamma']$*vs.* θ curve at the rotation center. The comparison between Fig. 13a and b also demonstrates the independence of the spring model on the pile diameter.

4.2. Relationship between foundation response and sand element response

Many existing studies show that there is analogous correspondence between soil response at element scale and foundation response at full scale. For example, Atkinson (2000) and Johansson et al. (2020) proved the close relationship of soil element response with the (non-linear) settlement and rocking stiffness of shallow foundations. Similarly, Bransby (1999) and Zhang and Andersen (2017) showed that the load transfer curves of laterally loaded piles can be scaled from the non-linear stress-strain curves of soil. Consequently, Wang et al. (2022c) investigated the soil stress-strain response and the rotational spring response in the FE simulations and identified that there is a one-to-one correspondence between the modulus degradation curves of sand (i.e., G/G_0-γ, where G_0 is the elastic modulus of sand, G is the secant modulus, γ is the shear strain) and the rotational stiffness degradation of the rigid piles ($K_R/K_{R,0}$ - θ, where $K_{R,0}$ is the initial rotational stiffness of rigid piles, $K_R = M_R/\theta$ is the secant rotational stiffness of rigid piles, θ is the pile rotation).

4.3. Determination of small strain (elastic) rotational stiffness, $K_{R,0}$

To define the rotational spring curve of the rigid pile in sand, it is necessary to establish the relationship between the initial rotational stiffness ($K_{R,0}$) and the small strain elemental shear modulus (G_0). Therefore, Wang et al. (2022c) performed a comprehensive series of elastic simulations on rigid monopiles with a wide range of configurations and interface roughness in soils with varying profiles of small strain elemental shear modulus (G_0). Based on statistical analyses of the computations, it was found the following format can best represent the relationship between $K_{R,0}$ and G_0:

$$K_{R,0} = C_k DL^2 G_{0.75L} \quad (5)$$

where $G_{0.75L}$ is the reference in-situ G_0 value at the rotation point and C_k

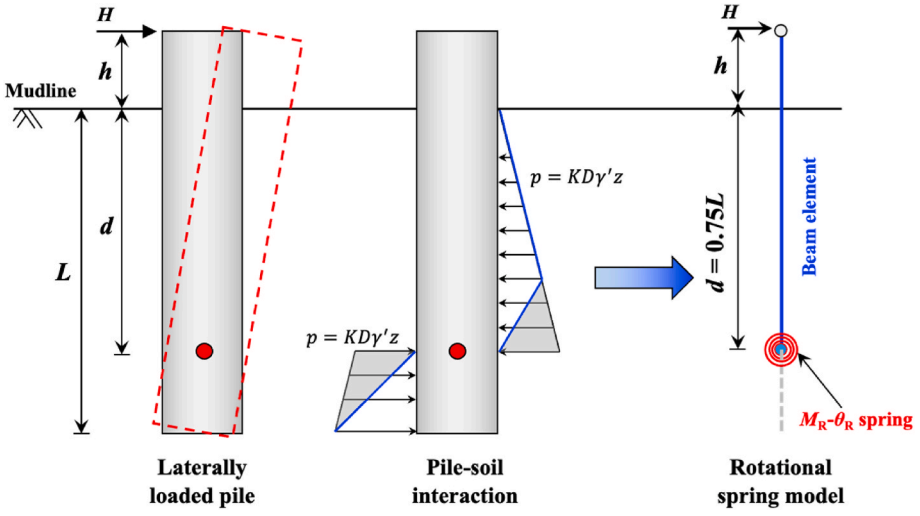

Fig. 12. The simplifed pile-soil interaction model and the proposed simple rotational spring model (Note: the soil resistance in the grey areas act in opposite directions and will cancel out each other relative to the rotation center. The blue line represents the equivalent net distribution.).

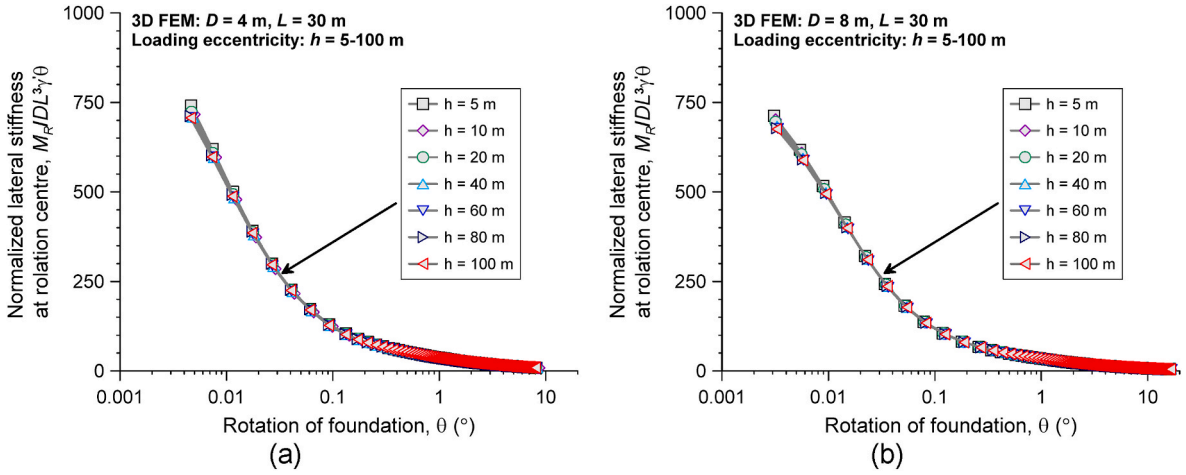

Fig. 13. Validation of the rotation spring model against FE simulations (D_r = 65%): (a) $[M_R/\theta DL^3\gamma']$*vs.* θ of 4 m diameter piles; (b) $[M_R/\theta DL^3\gamma']$*vs.* θ of 8 m diameter piles.

is a coefficient that varies primarily with L/D and the form of the G_0 profile.

The computed values of C_k of all simulations are summarized in Fig. 14 and fitted with explicit equations. Considering that G_0 of sand usually varies with the square root of the stress level, it may be inferred from this figure that $K_{R,0}$ can be taken as approximately $2.5DL^2G_{0.75L}$ for rigid piles with $2 \leq L/D \leq 5$ in uniform sand deposits.

4.4. Relationship for rotational stiffness outside of elastic range

The following modified hyperbolic function provides a good representation of the nonlinear degradation of the normalized secant shear modulus (G/G_0) of sand with shear strain (γ) (Fahey and Carter, 1993; Darendeli, 2001):

$$\frac{G}{G_0} = \frac{1}{1+(\gamma/\gamma_r)^a} \tag{6}$$

where a is the parameter controlling the degradation rate, and γ_r is the reference strain value. Studies also show that the shear stiffness of sand degrades more rapidly with shear strain at lower stress levels (Ishibashi and Zhang, 1993). Stokoe et al. (1995) found soil data over a wide range of stress levels can be unified when the reference strain was assumed to be proportional to the square root of the stress level. The hypoplastic model used to show the correspondence between elemental response and lateral pile response in Wang et al. (2022c) and described above employs a constant value of γ_r with $a = 1$ and hence could not be used directly to determine a relationship for pile rotational stiffness, K_R. Instead, new data from 26 rigid pile tests (as summarized in Table 1) are compiled in this study.

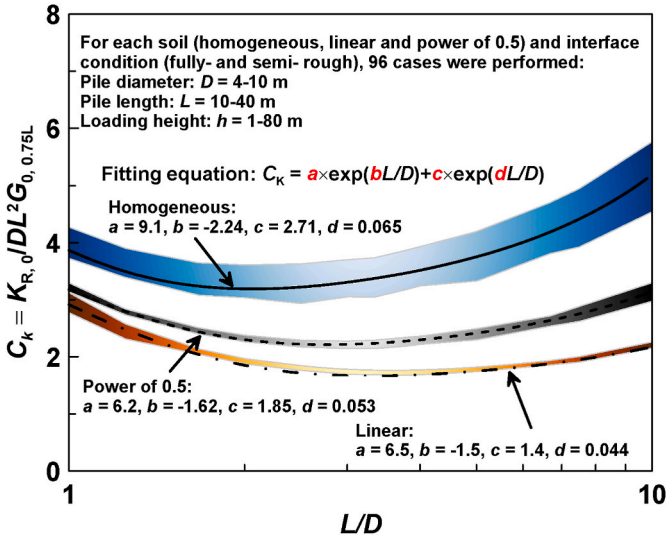

Fig. 14. Computed C_k values and predictions obtained using Eq. (5).

The database of rigid piles included small-scale centrifuge tests (Klinkvort and Hededal, 2014; Richards et al., 2021; Li et al., 2022) and reduced-scale field tests (Li et al., 2014; Wang et al., 2020; Belpile, 2020) covering piles with diameters (D) of 0.127–5.0 m, aspect ratios (L/D) of 2.2–7.9 and loading eccentricity ratios (h/L) of 0.23–4.5. The results were reanalyzed using the rotational spring model framework and are presented in Fig. 15. The normalized rotational stiffness degradation curves of these rigid piles fall into a narrow range and the relationship can be captured by the following equation:

$$K_R \Big/ K_{R,0} = 1 \Big/ \left[1+\left(\theta/\theta_{ref}\right)^{0.7}\right] \tag{7a}$$

$$\theta_{ref} = 0.0002 \times \left(\gamma' L/p_{ref}\right)^{0.5}, \text{where } p_{ref} = 100\ kPa. \tag{7b}$$

Eq. (7) bears a close similarity to published relationships that employ Eq. (6) to describe the variation of shear modulus with shear strain, hence providing additional verification of the correspondence between elemental shear modulus and pile rotational stiffness.

Therefore, the non-linear moment-rotation response of a laterally loaded rigid pile in sand can be approximated by combining Eq. (5) with Eq. (7). It is noted that Eq. (7) is derived from new back-analyses of tests of rigid or almost rigid piles and therefore the results are not affected by pile flexibility (which is discussed in the next section).

5. What is the influence of flexural rigidity for a monopile ?

Monopiles have been assumed to respond in a fully rigid mode in Sections 3 and 4. This means that the pile rotation at the rotation center is equal to that at the mudline without the extra contribution from pile bending. Monopiles used for offshore wind turbines are commonly assumed to behave in a rigid fashion (at least at large displacements) due to their low aspect ratios. This assumption is examined here noting that actual steel monopiles employed in the field have a finite flexural rigidity with typical diameter to wall thickness ratios (D/t, t is pile wall thickness) of between 60 and 120.

Fig. 16 presents the FE-calculated deflected shape of a typical 6 m diameter, 30 m long steel monopile with a wall thickness of 66 mm (giving $D/t = 91$) in medium dense sand (D_r = 60%) and that of a fully

Table 1
Summary of rigid pile tests in the literature.

Reference	Test No.	D (m)	L/D	h/L	$G_{0,\ 0.75L}$ (MPa)	$K_{R,\ 0}$ (MNm/rad)
Klinkvort and Hededal (2014)	Test K1	3	6	0.42	114.4	2.82×10^5
	Test K5	3	6	1.38	111.3	2.75×10^5
	Test K3	3	6	1.75	115.2	2.84×10^5
	Test K4	3	6	2.13	110.5	2.73×10^5
	Test K5	3	6	2.50	110.5	2.73×10^5
	Test K6	3	6	2.88	109.7	2.71×10^5
Wang et al. (2020)	Test W1	0.127	7.87	0.34	60.3	1.52×10^1
	Test W2	0.169	5.92	0.34	60.3	1.85×10^1
	Test W3	0.169	8.88	0.23	70.7	5.57×10^1
	Test W4	0.273	2.75	0.45	51.4	1.33×10^1
	Test W5	0.273	3.66	0.34	60.3	2.75×10^1
	Test W6	0.273	5.49	0.23	70.7	7.75×10^1
	Test W7	0.457	2.19	0.34	60.3	4.92×10^1
	Test W8	0.457	3.28	0.23	70.7	1.21×10^1
Richards et al. (2021)	Test R1	0.042	4	2.5	11.1	2.20×10^{-2}
	Test R2	0.378	4	2.5	33.3	4.85×10^1
	Test R3	3.36	4	2.5	99.2	1.02×10^5
Li et al. (2022)	Test L1	5	3	3.3	81.7	1.54×10^5
	Test L2	5	5	1	105.5	5.77×10^5
	Test L3	5	5	3	105.5	5.77×10^5
	Test L4	5	5	2	105.5	5.77×10^5
Li et al. (2014)	Test L1#	0.34	6.5	0.18	200	6.13×10^1
Belpile (2020)	Test B1	0.6	5.8	0.043	93.9	1.25×10^3
	Test B2	0.6	5.8	0.043	93.9	1.25×10^3
	Test B3	0.6	5.8	0.057	93.9	1.25×10^3
	Test B4	0.6	5.8	0.057	93.9	1.25×10^3

rigid pile with the same geometric configuration with loads applied to produce the same rotation at mudline (of 0.11°, 0.25° and 0.51°). The pile lateral response up to a rotation of 0.5° at mudline is considered as this rotation is a typical serviceability limit for monopiles.

Bending of the monopile can be identified from the pile deflection profiles in Fig. 16a, although it should be noted that the zero lateral displacement depth of the pile is still at around 0.75L. The pile bending is more apparent from the rotations plotted on Fig. 16b where it is evident that the rotation of the monopile increases with increasing distance above the pile tip. For a mudline pile rotation of 0.25°, the corresponding rotation angle of the monopile at the rotation center is less than 0.02° while the same value of 0.25° is shown for the rigid pile. It is clear that flexural rigidity has a significant influence on the pile deflection profile for a given mudline rotation and needs to be considered in design.

The formulations presented previously for a rigid pile can be

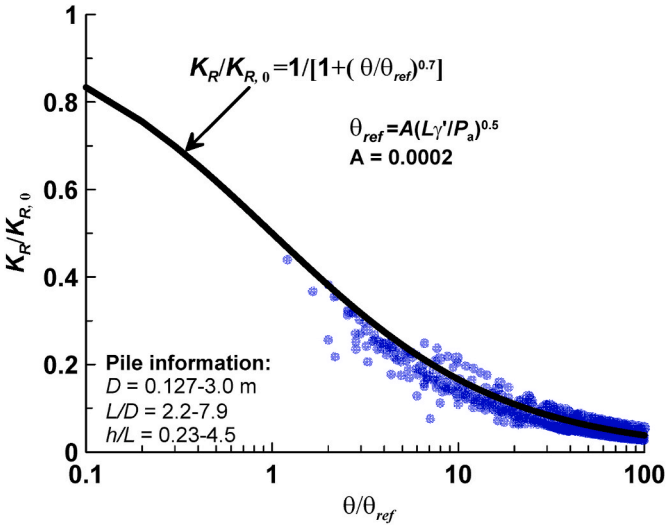

Fig. 15. $K_R/K_{R,\ 0}$ *vs.* θ/θ_{ref} for 25 pile tests at four sand sites.

adjusted to account for the extra pile rotation ($\Delta\ \theta$) arising from pile flexibility, as shown in Fig. 17. As this extra pile rotation is from pile bending, an estimate of $\Delta\theta$ can be found by calculating the mudline bending rotation ($\Delta\theta_F$) of a pile held rigidly at its rotation center (at a depth of 0.75L) and then dividing by a correction factor ($C_{R,\theta}$) to account for the different bending moment profile in the soil. The same procedure can be applied to correct for the displacement. As shown in Fig. 17, the surface rotation and displacement of a pile in air and fixed at a depth of 0.75L can be calculated from the bending moment profile as:

$$\Delta\theta_F = \int_0^{0.75L} M(z)dz \Big/ EI = \frac{H(2h+0.75L)\times 0.75L}{2EI} \tag{8a}$$

$$\Delta y_F = \iint_0^{0.75L} M(z)dzdz \,/\, EI = \frac{H(0.75L)^2[3\times(h+0.75L)-0.75L]}{6EI} \tag{8b}$$

where $M(z)$ is the distribution of bending moment along the pile, E is the Young's modulus of the pile material and I is the second moment of area of the monopile cross-section.

The monopile response in sand at each load level can then be calculated as follows (noting that the rotation and displacement of a rigid pile, θ_{rigid} and y_{rigid}, are determined using Eqs. (5) and (7)):

$$\theta_{Monopile} = \theta_{Rigid} + \Delta\theta_F / C_{R,\theta} \tag{9a}$$

$$y_{Monopile} = y_{Rigid} + \Delta y_F / C_{R,y} \tag{9b}$$

To determine the value of $C_{R,\ \theta}$ and $C_{R,\ y}$, additional 80 new finite element simulation cases involving five pile diameters (D) from 4 m to 10 m, twelve different aspect ratios (L/D) from 2 to 7.5 and thirteen loading eccentricity ratios (h/L) of 0.02–2.67 were performed using the same hypoplastic sand model adopted in Wang et al. (2022b). The analysis indicated that $C_{R,\ \theta}$ could be described almost exactly as a function of the loading eccentricity ratio (h/L) and was independent of the pile flexibility, pile diameter, pile length and sand density, while $C_{R,\ y}$ was equal to $1.75C_{R,\ \theta}$. The individual FE-calculated $C_{R,\ \theta}$ values are presented on Fig. 18 and are represented well by:

$$C_{R,\theta} = \frac{0.75\times\left[3\times 2.8+(h/L)^{0.75}\right]}{2.8+(h/L)^{0.75}} \tag{10}$$

To illustrate the suitability of employing Eqs. (8) and (9) to account for the effect of monopile flexibility, Fig. 19 presents results from the FE computed moment-rotation relationships for both rigid and flexible piles with different diameters and load eccentricities. A much softer response

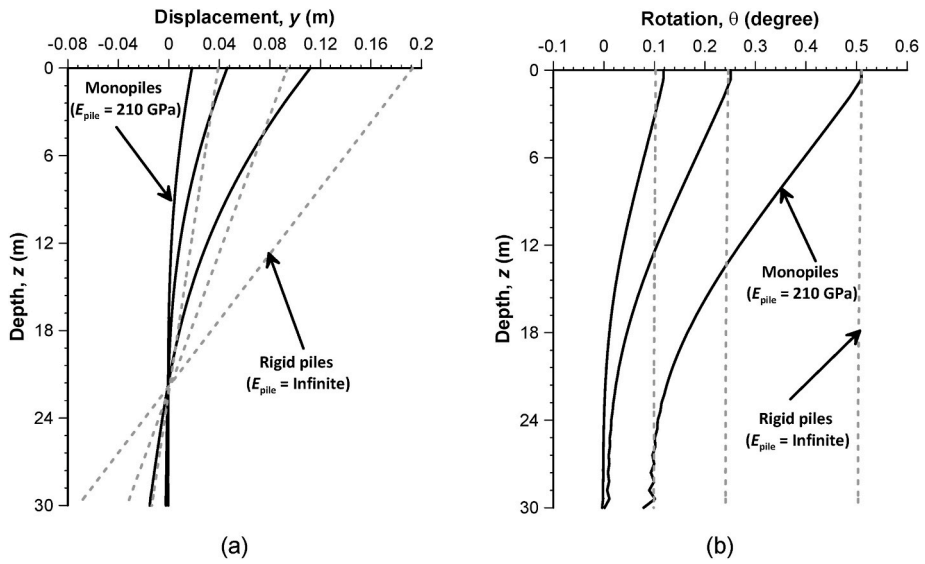

Fig. 16. Pile displacement and rotation profiles at different loads: (a) displacement profiles; (b) rotation profiles (Note: D = 6 m, L = 30 m, t = 0.06635 m).

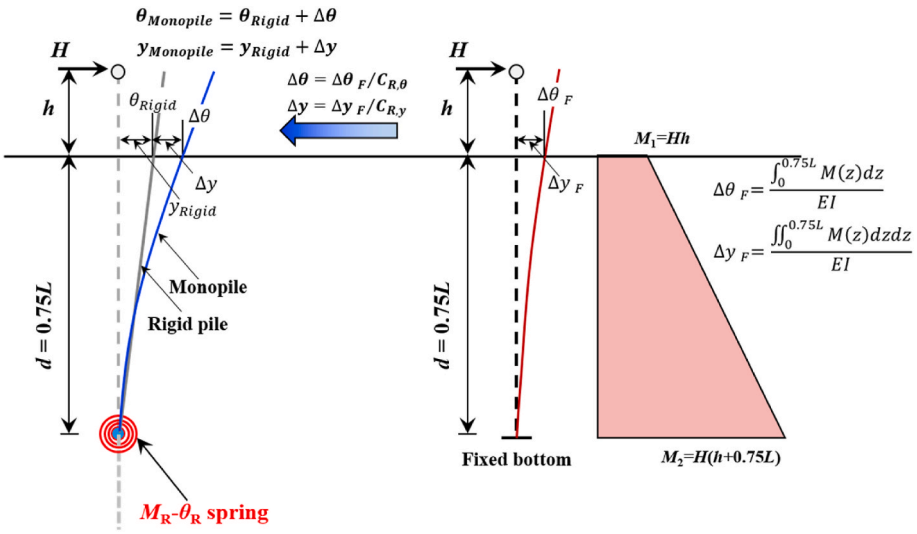

Fig. 17. Illustration of the correction for pile rigidity.

is evident for the monopile with a realistic configuration, illustrating the importance of pile flexibility. Fig. 19 also shows the responses calculated by adding the additional rotation ($\Delta\theta$) determined using Eq. (8) (where $C_{R,\theta}$ is determined from Eq. (10)) to the rotation computed for a rigid pile at the same moment. It is evident that this approach is successful in accounting for the additional flexibility of monopiles on the moment-mudline rotation response.

To further validate the proposed bending correction method (Eqs. (8)–(10)) and the empirical equations for the nonlinear degradation of foundation stiffness (Eq. (5) and Eq. (7)), the field tests performed by the PISA (Pile–Soil Analysis) joint industry project in dense sand at Dunkirk (McAdam et al., 2020) were back-analyzed. The test piles had diameters (D) of 0.273 m, 0.762 m and 2.0 m with aspect ratios (L/D) in the range of 2.9–8 and loading eccentricities (h/L) from 0.9 to 4.5. According to the analysis of the measured bending moment and pile displacement data, bending of the tested piles due to the finite pile rigidity was reported in McAdam et al. (2020). Details of the tests analyzed in this study are summarized in Table 2.

Fig. 20 presents the measured and back-calculated load-deflection response of the field tests in the PISA project. As shown in the figure, the responses of different diameter monopiles can be well predicted by the rotational spring model and the proposed empirical equations, especially at small deflections related to monopile foundation design for offshore wind turbines. The good agreement between the test results and model predictions demonstrates the reliability of the rotational spring model (Eq. (5) and Eq. (7)) and the pile flexural rigidity correction method (Eqs (8)–(10)).

Summarizing the results in Section 3, 4 and 5, it is clear that the nonlinear moment-rotation response of a laterally loaded monopile in uniform sand can be easily obtained from the proposed simple rotational spring model. The model is anchored to centrifuge and field pile testing data, and encapsulates the rotational mechanism of monopiles in a single spring as well as the effect of pile flexural rigidity. Compared with the existing design approach (e.g. p-y load transfer method), the developed model does not need to define multiple lateral, distributed moment and pile base springs to achieve an acceptable solution (as in Byrne et al., 2015; Wang et al., 2020). It can be applied easily in preliminary soil-structure interaction analyses and integrated simply in structural dynamic analyses. To allow the easy use of the model, a step-by-step flow chart containing the equations is provided in Fig. 21.

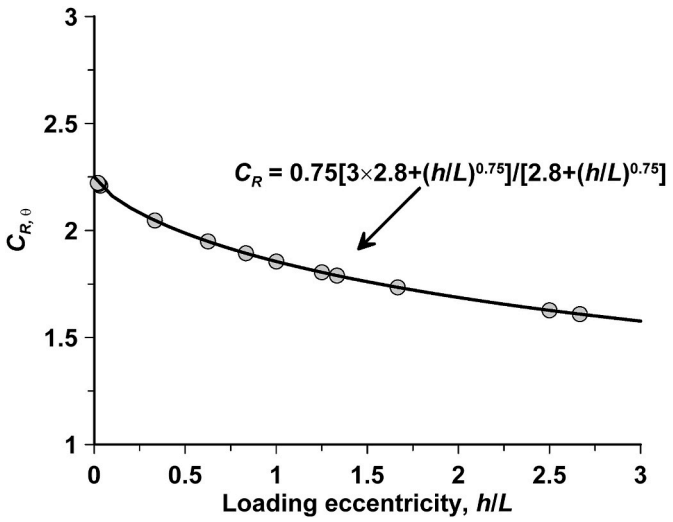

Fig. 18. The relationship between the correction factor ($C_{R,\theta}$) and the loading eccentricity ratio (h/L); Note: simulations indicated no dependence of $C_{R,\theta}$ on D or L/D and so many of the data points overlap.

6. Example application of the rotational spring model to design

In this section, a typical monopile supporting a 10 MW offshore wind turbine (OWT) is selected as an example to show the usefulness and simplicity of the proposed rotational spring model in foundation design and the structural dynamic analysis of OWTs. The key parameters of the OWT are summarized in Table 3 (Velarde, 2016). The loads from wind, wave and current are equivalent to a horizontal force applied at a loading eccentricity (h) of 50 m above the seabed surface. The ground comprises sand with an estimated elastic shear modulus profile given by:

Table 2
Key features of piles and sand in tests of McAdam et al. (2020).

Test NO.	Test M1	Test M2	Test M3	Test M4	Test M5	Test M6
D (m)	0.273	0.273	0.762	0.762	2.0	2.0
t (m)	0.007	0.007	0.01	0.01	0.038	0.038
L (m)	1.43	2.18	2.24	3.98	10.61	10.57
L/D	5.24	8	2.94	5.22	5.31	5.29
h/L	3.5	2.3	4.46	2.51	0.93	0.94
$G_{0,\ 0.75L}$ (MPa)	70	70	70	83	120	120
C_k	3.81	4.55	3.29	3.81	3.83	3.82
$K_{R,\ 0}$ (MNm/rad)	149	413	881	3812	103365	102454
$C_{R,\theta}$	2.68	2.89	2.56	2.85	3.27	3.27

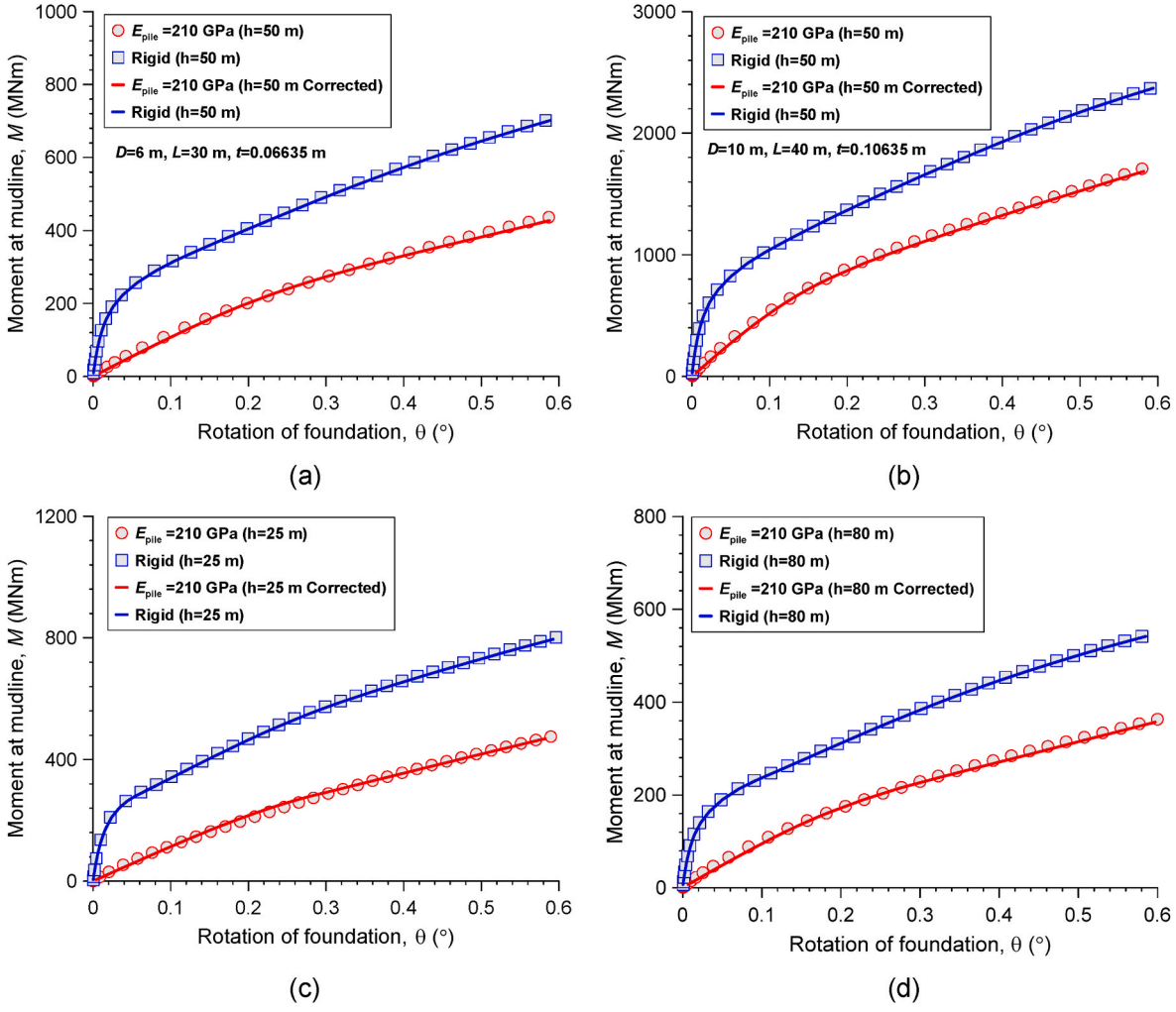

Fig. 19. Comparison of moment-rotation response at mudine before and after correction for different piles: (a) $D = 6$ m, $L/D = 5$, $h/L = 1.67$, $D/t = 91$, $C_{R,\theta} = 1.73$; (b) $D = 10$ m, $L/D = 3$, $h/L = 1.67$, $D/t = 94$; $C_{R,\theta} = 1.73$; (a) $D = 6$ m, $L/D = 5$, $h/L = 2.67$, $C_{R,\theta} = 1.61$, $D/t = 91$; (b) $D = 10$ m, $L/D = 4$, $h/L = 0.625$, $C_{R,\theta} = 1.61$, $D/t = 94$.

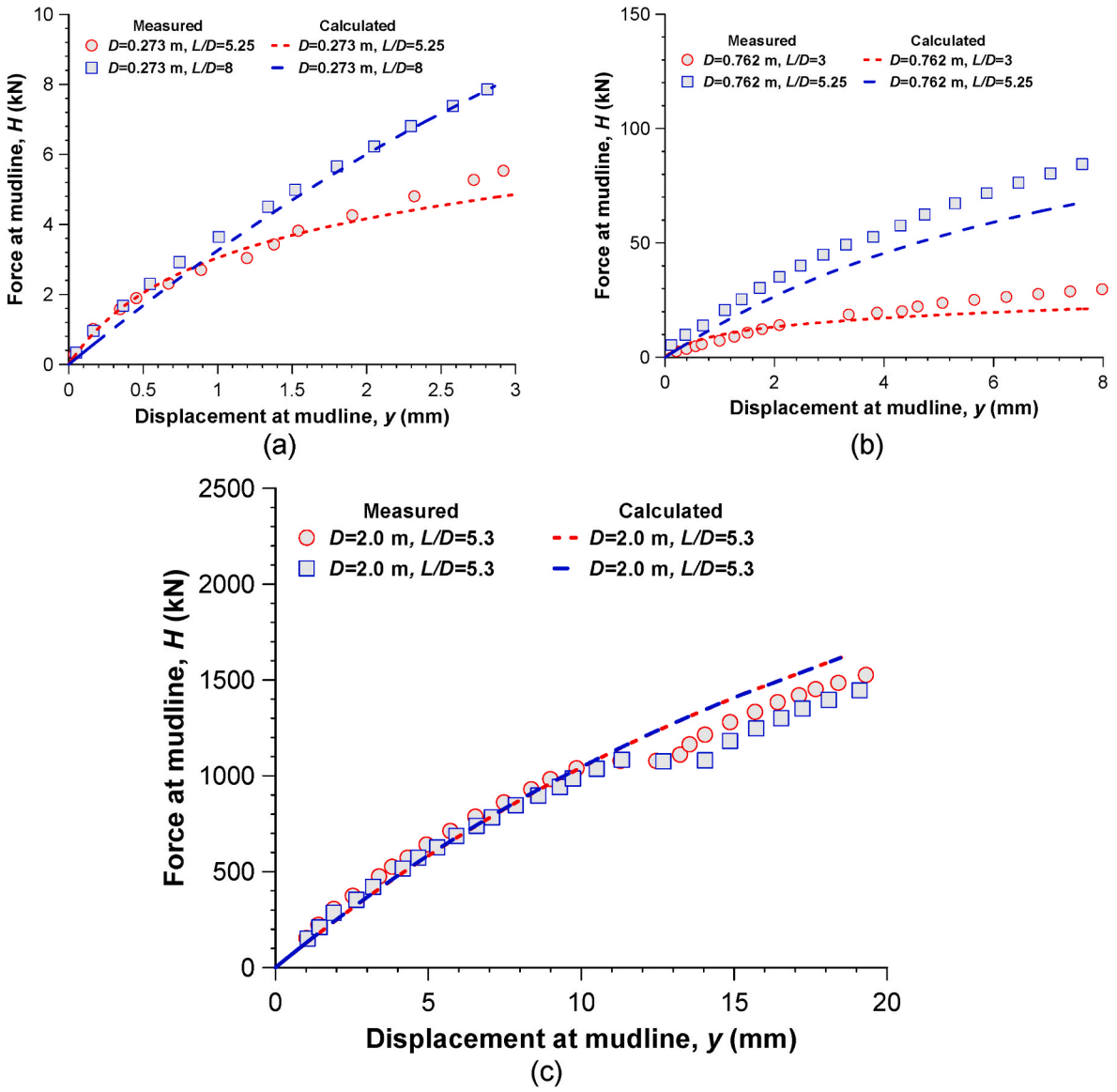

Fig. 20. Comparison of the measured and calculated load-defelction response of pile tests in PISA project: (a) $D = 0.273$ m; (b) $D = 0.762$ m; (c) $D = 2.0$ m.

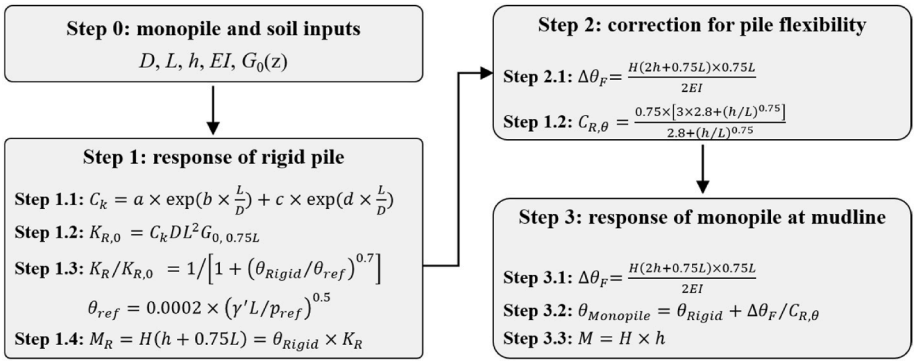

Fig. 21. Flow chart indicating the steps for calculating the moment-rotation response of monopiles.

G_0 (MPa) = 20 [z (m)]$^{0.5}$, as shown in Fig. 22b.

1. The first step is to calculate the shear modulus at the depth of the rotation center $G_{0,\ 0.75L}$ (MPa) = 20 × (35 × 0.75)$^{0.5}$ = 102.5 MPa.
2. Then, according to the elastic foundation stiffness equations in Fig. 14, the value of C_k can be calculated as $C_k = 6.2 \times \exp(-1.62 \times 35/10) + 1.85 \times \exp(0.053 \times 35/10) = 2.2$. Alternatively, as explained above, a C_k value of 2.5 can be used without any significant loss in accuracy.

Table 3
Input parameters of the DTU-10 MW OWT (Velarde, 2016).

DTU-10 MW Key Parameters	Value
Rated power, (MW)	10
Tower height, L_T (m)	115.63
Tower top diameter, D_t (m)	7
Tower bottom diameter, D_b (m)	10.5
Tower wall thickness, t_T (mm)	20–38
Top mass, m_t (t)	674
Substructure height, L_s (m)	40
Substructure diameter, D_s (m)	10.5
Monopile depth, L_p (m)	35
Monopile diameter, D_p (m)	10
Monopile wall thickness, t_p (mm)	120
Monopile aspect ratio, L/D	3.5
Structure stiffness, E (GPa)	210
Structure density, $\rho_{\pi\lambda\varepsilon}$ (kg/m^3)	8500
Effective soil unit weight, γ_{soil} (kN/m^3)	10
Shear modulus of the soil at rotation center, $G_{0,\ 0.75L}$ (MPa)	102.5
Rotational stiffness coefficient, C_k	2.2
Initial stiffness of rotational spring, $K_{R,0}$ (Nm/rad)	2.82E+12

3. Therefore, the initial rotational stiffness $K_{R,\ 0} = C_k D L^2 G_{0,\ 0.75L} = 2.2 \times 10 \times 35^2 \times 102.5 = 2.82 \times 10^6$ MNm/rad.
4. The secant stiffness of the rotational spring for a rigid pile at any rotation, θ, can be obtained by using $K_{R,\ 0}$ in Eq. (5): $K_R = M_R/\theta D L^3 \gamma' = K_{R,0} \times 1/\{1+[\theta/(0.0002 \times (10 \times 35/100)^{0.5})]^{0.7}\} = 2.82 \times 10^6/[1+(\theta/3.74 \times 10^{-4})^{0.7}]$
5. In this case, considering $M_R = H(h+0.75L) = \theta \times K_R$, the moment response at mudline can be also easily calculated as $M = h/(h+0.75L) \times \theta K_R$.
6. Finally, the rotation should be corrected by including the extra value from pile bending $\Delta\theta = \Delta\theta_F/C_{R,\theta}$, where $\Delta\theta_F = H(h + h+0.75L) \times 0.75L/2EI$, $H = M/h$, and $C_{R,\theta} = 0.75 \times [3 \times 2.8+(50/35)^{0.75}]/[2.8+(50/35)^{0.75}] = 1.77$.
7. The resulting moment-rotation response at the mudline is presented in Fig. 23a.

One typical application of the rotational spring model is to assist with rapid determination of the natural frequency of an offshore wind turbine. To illustrate this application, a beam-spring model of a typical OWT was built in Abaqus, where the soil was represented by the calculated nonlinear rotational spring at a depth of 0.75L. 3D beam elements ('B31') were used to model the monopile and turbine tower, while 'Spring1' element in Abaqus was adopted to model the nonlinear soil spring. The blade, hub, and nacelle weights were simulated by adding a point mass at the tower head. An eigenvalue analysis using the linear perturbation method was then performed using the built-in 'Frequency' function in Abaqus. Fig. 23b presents the computed natural frequencies of the turbine at different monopile rotations. It is seen that the whole system has a natural frequency of around 0.25 Hz when the foundation rotation is small and its response is governed by the elastic stiffness. However, due to the soil nonlinearity shown in Fig. 23a, the foundation stiffness decreases with increasing rotation, leading to a lower system natural frequency, as shown in Fig. 23b. For example, the natural frequency at a pile rotation of 0.25° is 0.23 Hz which is 8% smaller than the value of 0.25 Hz at low rotations.

7. Summary

This paper presents a synthesis of recent and new research on laterally monotonically loaded monopiles in drained sand, which involved field tests, centrifuge model tests and finite element simulations. The study was motivated by questions concerning the contribution of the pile base to resistance, the relevance (or otherwise) of the API p-y model and the need for a simple approach that can be employed in soil-structure interaction analyses for preliminary design.

The paper has demonstrated that:

(i) The contribution of pile base resistance (i.e., base shear force and moment) to the lateral response of monopiles in drained sand is negligible for the conditions investigated.
(ii) The API p-y model is not suitable for prediction of the lateral response of rigid monopiles in sand largely because of the inappropriateness of the specified initial stiffness and stiffness degradation characteristic.
(iii) The normalized net pressure curves (p/D-y/D) and the soil pressure ($P_u = p_u/D$) at ultimate capacity are independent of the pile diameter (D) and load eccentricity (h).
(iv) The profile of net pressure of a rigid pile at all levels of lateral loading can be approximated as the simplified pile-soil interaction model originally proposed by Petrasovits and Award (1972).
(v) A correspondence exists between the elemental shear modulus of the sand (G_0) and the initial pile rotational stiffness ($K_{R,0}$).
(vi) The flexibility of monopiles has to be considered in design at small pile displacements.

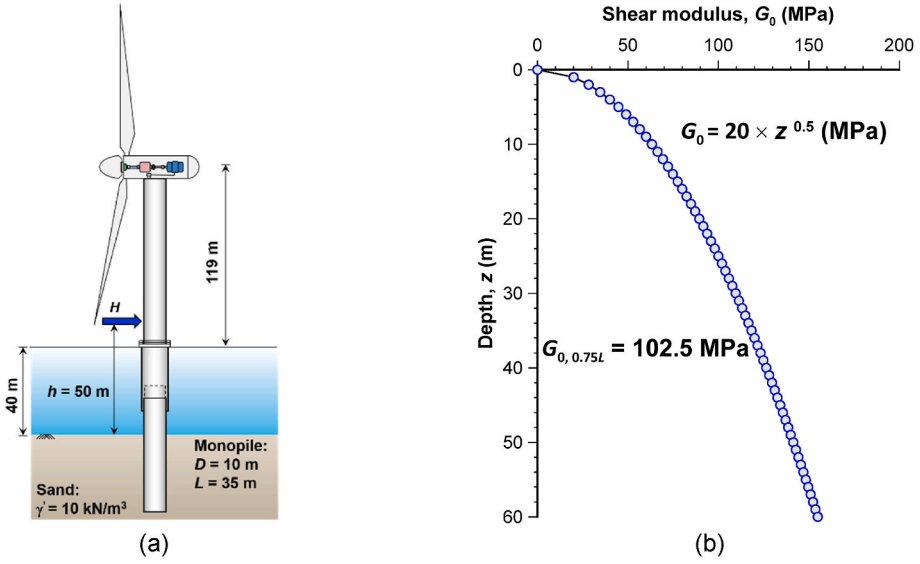

Fig. 22. Design inputs of the example application: (a) offshore wind turbine supported by monopile (D = 10 m, L = 35 m); (b) nonhomogeneous small strain soil shear modulus profile (G_0).

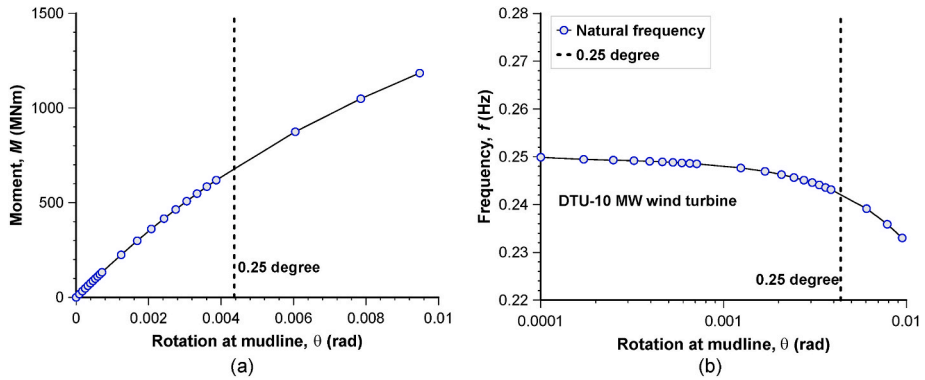

Fig. 23. Calculated monopile response using the proposed simple model: (a) the moment-rotation response; (b) the natural frequency of OWT at different rotations.

Based on these findings, a simplified approach is proposed to model the nonlinear response of a monopile as a rigid beam hinged at the rotation center at a depth of 0.75L with movement constrained by a rotational spring of stiffness K_R and then allowing separately for pile bending. The rotational spring stiffness for a rigid pile at very low pile rotations ($K_{R,0}$) can be established using a new correlation with the in-situ soil small strain shear modulus (G_0), while the rate of degradation of rotational stiffness (K_R) as the rotation (θ) increases is developed using the newly compiled data measured in lateral load tests on 26 rigid piles. A new simple method of correcting the expression for K_R to account for the flexibility of monopiles is finally derived and shown to be consistent with both FE simulations of flexible monopiles and (flexible) test piles performed in the PISA project (McAdam et al., 2020). An example illustrating application of the proposed approach for an offshore wind turbine is provided to demonstrate the simplicity and efficiency of the model.

CRediT authorship contribution statement

H. Wang: Conceptualization, Methodology, Validation, Formal analysis, Investigation, Writing – original draft, Visualization. **B.M. Lehane:** Conceptualization, Methodology, Investigation, Resources, Supervision, Writing – review & editing. **M.F. Bransby:** Conceptualization, Methodology, Investigation, Resources, Supervision, Writing – review & editing, Funding acquisition. **L.Z. Wang:** Resources, Writing – review & editing. **Y. Hong:** Writing – review & editing. **A. Askarinejad:** Writing – review & editing.

Declaration of competing interest

The authors declare that they have no known competing financial interests or personal relationships that could have appeared to influence the work reported in this paper.

Data availability

Data will be made available on request.

Acknowledgements

The third author holds the Fugro Chair in Geotechnics, whose support is gratefully acknowledged.

References

Achmus, M., Albiker, J., Peralta, P., Tom Wörden, F., 2011. Scale effects in the design of large diameter monopiles. EWEA, Brussels, pp. 326–328, 14 - 17 March.
Alderlieste, E.A., 2011. Experimental Modelling of Lateral Loads on Large Diameter Monopile Foundations in Sand. M.Sc. Thesis. Delft University of Technology.
Amar Bouzid, D., 2018. Numerical investigation of large-diameter monopiles in sands: critical review and evaluation of both API and newly proposed *p-y* curves. Int. J. GeoMech. 18 (11), 04018141.
API (American Petroleum Institute), 2011. Geotechnical and Foundation Design Considerations. API RP 2GEO, Washington, DC: API.
Ashford, S.A., Juirnarongrit, T., 2003. Evaluation of pile diameter effect on initial modulus of subgrade reaction. J. Geotech. Geoenviron. Eng. 129 (3), 234–242.
Ashour, M., Helal, A., 2013. Contribution of vertical skin friction to the lateral resistance of large-diameter shafts. J. Bridge Eng. 19 (2), 289–302.
Atkinson, J.H., 2000. Non-linear soil stiffness in routine design. Geotechnique 50 (5), 487–508.
Belpile, 2020. Lateral Pile Tests for the Equinix PE3 Project, 1/28. Guthrie Street, Osborne Pk, WA 6017, Australia.
Bransby, M.F., 1999. Selection of *p-y* curves for the design of single laterally loaded piles. Int. J. Numer. Anal. Methods GeoMech. 23 (15), 1909–1926.
Byrne, B.W., Mcadam, R., Burd, H.J., Houlsby, G.T., Martin, C.M., Zdravkovic, L., Taborda, D.M.G., Potts, D.M., Jardine, R.J., Sideri, M., Schroeder, F.C., Gavin, K., Doherty, P., Igoe, D., Muir Wood, A., Kallehave, D., Skov Gretlund, J., 2015. New design methods for large diameter piles under lateral loading for offshore wind applications. In: 3rd International Symposium on Frontiers in Offshore Geotechnics - ISFOG, pp. 705–710. Oslo, Norway.
Burd, H.J., Taborda, D.M., Zdravković, L., Abadie, C.N., Byrne, B.W., Houlsby, G.T., et al., 2020. PISA design model for monopiles for offshore wind turbines: application to a marine sand. Geotechnique 70 (11), 1048–1066.
Carter, D.P., 1984. A Non-linear Soil Model for Predicting Lateral Pile Response. PhD Thesis. Technical University of Auckland.
Choo, Y.W., Kim, D., 2015. Experimental development of the *p-y* relationship for large-diameter offshore monopiles in sands: centrifuge tests. J. Geotech. Geoenviron. Eng. 142 (1), 04015058.
Choo, Y.W., Kim, D., Park, J.H., Kwak, K., Kim, J.H., Kim, D.S., 2014. Lateral response of large-diameter monopiles for offshore wind turbines from centrifuge model tests. Geotech. Test J. 37 (1), 107–120.
Doherty, P., Gavin, K., 2012. Laterally loaded monopile design for offshore wind farms. Proceedings of the Institution of Civil Engineers-Energy 165 (1), 7–17.
DNV, G.L., 2014. DNV-OS-J101–Design of Offshore Wind Turbine Structures. DNV GL, Oslo, Norway.
Darendeli, B.M., 2001. Development of a New Family of Normal-Ized Modulus Reduction and Material Damping Curves. PhD Thesis. University of Texas at Austin, TX, USA.
Fahey, M., Carter, J.P., 1993. A finite element study of the pressuremeter test in sand using a nonlinear elastic plastic model. Can. Geotech. J. 30 (2), 348–362.
Fan, C.C., Long, J.H., 2005. Assessment of existing methods for predicting soil response of laterally loaded piles in sand. Comput. Geotech. 32 (4), 274–289.
Finn, W.L., Dowling, J., 2015. Modelling effects of pile diameter. Can. Geotech. J. 53 (1), 173–178.
Fleming, K., Weltman, A., Randolph, M., Elson, K., 2008. Piling Engineering. CRC press.
Georgiadis, M., Anagnostopoulos, C., Saflekou, S., 1992. Centrifugal testing of laterally loaded piles in sand. Can. Geotech. J. 29 (2), 208–216.
Hong, Y., He, B., Wang, L.Z., Wang, Z., Ng, C.W.W., Mašín, D., 2017. Cyclic lateral response and failure mechanisms of semi-rigid pile in soft clay: centrifuge tests and numerical modelling. Can. Geotech. J. 54 (6), 806–824.
Hong, Y., Koo, C.H., Zhou, C., Ng, C.W., Wang, L.Z., 2016. Small strain path-dependent stiffness of Toyoura sand: laboratory measurement and numerical implementation. Int. J. GeoMech. 17 (1), 04016036.
Houlsby, G.T., 2016. Interactions in offshore foundation design. Geotechnique 66 (10), 791–825.
Ishibashi, I., Zhang, X., 1993. Unified dynamic shear moduli and damping ratios of sand and clay. Soils Found. 33 (1), 182–191.
Jeong, S., Kim, Y., Kim, J., 2011. Influence on lateral rigidity of offshore piles using proposed *p-y* curves. Ocean Eng. 38 (2–3), 397–408.
Johansson, J., Sivasithamparam, N., Zhang, Y.H., Engin, H.K., 2020. Simple method for computing nonlinear foundation rocking stiffness and damping. In: 4th International Symposium on Frontiers in Offshore Geotechnics. American Society of Civil Engineers, pp. 1824–1833.
Kallehave, D., Thilsted, C.L., Liingaard, M., 2012. Modification of the API *p-y* formulation of initial stiffness of sand. In: Proceedings of Offshore Site Investigation and

Geotechnics: Integrated Technologies-Present and Future. Society of Underwater Technology, London, UK, pp. 465–472.
Kirkwood, P.B., 2016. Cyclic Lateral Loading of Monopile Foundations in Sand. Ph.D. Thesis. University of Cambridge.
Klinkvort, R., Page, A., 2014. Diameter effect on the lateral response of monopiles in sand supporting offshore wind turbines. In: 8th European Conference on Numerical Methods in Geotechnical Engineering, pp. 1267–1272.
Klinkvort, R.T., Hededal, O., 2014. Effect of load eccentricity and stress level on monopile support for offshore wind turbines. Can. Geotech. J. 51 (9), 966–974.
Klinkvort, R.T., 2012. Centrifuge Modelling of Drained Lateral Pile - Soil Response: Application for Offshore Wind Turbine Support Structures. Ph.D. Thesis. Technical University of Denmark.
Lam, I.P., Martin, G.R., 1986. Seismic Design of Highway Bridge Foundations. Design Procedures and Guidelines, 2. U.S. Department of Transportation, Federal Highway Administration, Springfield, Virginia, U.S.A. Report No. FHWA/RD-86/102.
Lesny, K., Wiemann, J., 2006. Finite-element-modelling of large diameter monopiles for offshore wind energy converters. In: Proceedings of Geo Congress, Atlanta, GA. ASCE, Reston, VA, pp. 1–6.
Leth, C.T., 2013. Improved Design Basis for Laterally Loaded Large Diameter Pile: Experimental Based Approach: Revised Version. River Publishers.
Li, W., Zhu, B., Yang, M., 2017. Static response of monopile to lateral load in overconsolidated dense sand. J. Geotech. Geoenviron. Eng. 143 (7), 04017026.
Li, W., Igoe, D., Gavin, K., 2014. Evaluation of CPT-based *P–y* models for laterally loaded piles in siliceous sand. Géotech. Lett. 4 (2), 110–117.
Li, Z.S., Blanc, M., Thorel, L., 2022. Effects of embedding depth and load eccentricity on lateral response of offshore monopiles in dense sand: a centrifuge study. Geotechnique 1–15.
Liang, R., Shatnawi, E.S., Nusairat, J., 2007. Hyperbolic *p-y* criterion for cohesive soils. Jordan Journal of Civil Engineering 1 (1), 38–58.
Mathew, G.V., Lehane, B.M., 2012. Numerical back-analyses of greenfield settlement during tunnel boring. Can. Geotech. J. 50 (2), 145–152.
McAdam, R.A., Byrne, B.W., Houlsby, G.T., Beuckelaers, W.J.A.P., Burd, H.J., Gavin, K., Igoe, D., Jardine, R.J., Martin, C.M., Muir Wood, A., Potts, D.M., Skov Gretlund, J., Taborda, D.M.G., Zdravkovid, 2020. Monotonic laterally loaded pile testing in a dense marine sand at Dunkirk. Geotechnique 1–13.
Murff, J.D., Hamilton, J.M., 1993. P-ultimate for undrained analysis of laterally loaded piles. Journal of Geotechnical Engineering 119 (1), 91–107.
Murphy, G., Igoe, D., Doherty, P., Gavin, K., 2018. 3D FEM approach for laterally loaded monopile design. Comput. Geotech. 100, 76–83.
Negro, V., López-Gutiérrez, J.S., Esteban, M.D., Alberdi, P., Imaz, M., Serraclara, J.M., 2017. Monopiles in offshore wind: preliminary estimate of main dimensions. Ocean Eng. 133, 253–261.
Petrasovits, G., Award, A., 1972. Ultimate lateral resistance of a rigid pile in cohesionless soil. In: Proc., 5th European Conf. On SMFE 3. The Spanish Society for Soil Mechanics and Foundation, pp. 407–412.
Pender, M.J., 2004. Discussion of "evaluation of pile diameter effect on initial modulus of subgrade reaction" by scott A. Ashford and terrawut Juirnarongrit. J. Geotech. Geoenviron. Eng. 130 (9), 981–982.
Poulos, H.G., 1971. Behavior of laterally loaded piles: I-single piles. J. Soil Mech. Found Div. 97 (5), 711–731.
Randolph, M.F., 1981. The response of flexible piles to lateral loading. Geotechnique 31 (2), 247–259.
Randolph, M.F., O'Neill, M.P., Erbrich, C., 1998. Performance of Suction Anchors in Fine-Grained Calcareous Soils. Proc. Offshore Tech. Conf., Houston paper 8831.
Richards, I.A., Bransby, M.F., Byrne, B.W., Gaudin, C., Houlsby, G.T., 2021. Effect of stress level on response of model monopile to cyclic lateral loading in sand. J. Geotech. Geoenviron. Eng. 147 (3), 04021002.
Reese, L.C., Cox, W.R., Koop, F.D., 1974. Analysis of laterally loaded piles in sand. Offshore Technology in Civil Engineering Hall of Fame Papers from the Early Years 95–105.
Sørensen, S.P.H., 2012. Soil-structure Interaction for Non-slender Large Diameter Offshore Monopoles. Ph.D. Thesis. Aalborg University, Aalborg, Denmark.
Stokoe, K.H., Hwang, S.K., Darendeli, M.B., Lee, N.J., 1995. Correlation study of nonlinear dynamic soils properties. Aiken, SC, Westinghouse Savannah River Company.
Thieken, K., Achmus, M., Lemke, K., 2015. A new static *p-y* approach for piles with arbitrary dimensions in sand. Geotechnik 38 (4), 267–288.
Velarde, J., 2016. Design of Monopile Foundations to Support the DTU 10 MW Offshore Wind Turbine. M.Sc. Thesis. NTNU.
Wan, X., Doherty, J.P., Randolph, M.F., 2021. Relationships between lateral and rotational load transfer stiffnesses and soil modulus for the elastic response of monopiles. Comput. Geotech. 137, 104256.
Wang, H., Lehane, B.M., Bransby, M.F., Wang, L.Z., Hong, Y., 2020. A simple CPT approach for predicting the ultimate lateral capacity of a rigid pile in sand. Géotech. Lett. 1–25.
Wang, H., Lehane, B.M., Bransby, M.F., Wang, L.Z., Hong, Y., 2022a. Field and numerical study of the lateral response of rigid piles in sand. Acta Geotechnica 1–12.
Wang, H., Bransby, M.F., Lehane, B.M., Wang, L., Hong, Y., 2022b. Numerical Investigation of the Monotonic Drained Lateral Behaviour of Large-Diameter Rigid Piles in Medium-Dense Uniform Sand. Géotechnique, pp. 1–12.
Wang, H., Lehane, B.M., Bransby, M.F., Askarinejad, A., Wang, L.Z., Hong, Y., 2022c. A simple rotational spring model for laterally loaded rigid piles in sand. Mar. Struct. 84, 103225.
Wang, H., Wang, L.Z., Askarinejad, A., Hong, Y., He, B., 2022d. Ultimate soil resistance of the laterally loaded pile in uniform sand. Can. Geotech. J. (ja).
Wiemann, J., Lesny, K., Richwien, W., 2004. Evaluation of Pile Diameter Effects on Soil-Pile Stiffness. University of Duisburg-Essen. Institute for Soil Mechanics and Foundation Engineering, Essen, Germany.
Zhang, Y., Andersen, K.H., 2017. Scaling of lateral pile *p-y* response in clay from laboratory stress-strain curves. Mar. Struct. 53, 124–135.
Zhu, B., Li, T., Xiong, G., Liu, J.C., 2016. Centrifuge model tests on laterally loaded piles in sand. Int. J. Phys. Model. Geotech. 16 (4), 160–172. PAGE * MERGEFORMAT 20 NUMPAGES * MERGEFORMAT 20.